

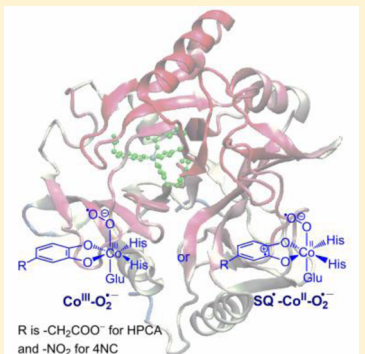
# Reaction Mechanism of Cobalt-Substituted Homoprotocatechuate 2,3-Dioxygenase: A QM/MM Study

Lili Cao, Geng Dong, and Wenzhen Lai\*

Department of Chemistry, Renmin University of China, Beijing, 100872, China

Supporting Information

**ABSTRACT:** The reaction mechanisms of cobalt-substituted homoprotocatechuate 2,3-dioxygenase (Co-HPCD) with electron-rich substrate homoprotocatechuate (HPCA) and electron-poor substrate 4-nitrocatechol (4NC) were investigated by quantum mechanical/molecular mechanical (QM/MM) calculations. Our results demonstrated that the Co-O<sub>2</sub> adducts has doublet ground state with a Co<sup>III</sup>-O<sub>2</sub><sup>•-</sup> character when 4NC was used as the substrate, in good agreement with the EPR spectroscopic experiment. The reactive oxygen species is the doublet Co<sup>III</sup>-O<sub>2</sub><sup>•-</sup> for Co-HPCD/4NC and the quartet SQ<sup>•+</sup>-Co<sup>II</sup>-O<sub>2</sub><sup>•-1</sup> species for Co-HPCD/HPCA, indicating that the substrate plays important roles in the dioxygen activation by Co-HPCD. B3LYP was found to overestimate the rate-limiting barriers in Co-HPCD. TPSSh predicts barriers of 21.5 versus 12.0 kcal/mol for Co-HPCD/4NC versus Co-HPCD/HPCA, which is consistent with the fact that the rate of the reaction is decreased when the substrate was changed from HPCA to 4NC.



## 1. INTRODUCTION

Catecholic dioxygenases catalyze the cleavage of the aromatic ring of the substrate with the incorporation of two atoms of dioxygen into the product, assisting in the degradation of aromatic compounds.<sup>1</sup> The active sites of these enzymes contain a metal center ligated by two histidines and one glutamate, which form a so-called 2-His-1-carboxylate facial triad, a motif found in many mononuclear nonheme iron enzymes that activate dioxygen.<sup>2,3</sup> Homoprotocatechuate 2,3-dioxygenases that catalyze the ring-opening of homoprotocatechuate (HPCA) are the most studied extradiol-cleaving catecholic dioxygenases.

The iron-containing homoprotocatechuate 2,3-dioxygenase from *Brevibacterium fuscum* (Fe-HPCD) and manganese-containing enzyme from *Arthrobacter globiformis* (Mn-MndD) have a remarkable structural similarity, suggested from their X-ray crystal structures.<sup>4,5</sup> In recent metal substitution experiments, the native Fe(II) metal cofactor of HPCD was substituted with Mn(II)<sup>5,6</sup> and Co(II),<sup>7</sup> leading to Mn-HPCD and Co-HPCD, and manganese in MndD, was swapped for iron to produce Fe-MndD.<sup>5</sup> It is surprising to find that four enzymes, Fe-HPCD, Mn-HPCD, Mn-MndD, and Fe-MndD, show nearly the same activity, while Co-HPCD exhibits catalytic activity even much higher than that for Fe-HPCD and Mn-HPCD under saturating O<sub>2</sub> conditions, though cobalt has the highest standard M(III/II) redox potential of the three metals (1.92, 1.56, and 0.77 V for the Co(III/II), Mn(III/II), and Fe(III/II) couples, respectively).<sup>8</sup> Moreover, the X-ray crystal structures of the resting and substrate-bound forms of Fe-HPCD, Mn-HPCD, and Co-HPCD show no significant structural differences in the active site environment, suggesting that the protein structure does not differentially tune the potential of the metal center.<sup>7</sup> These findings support the

previously proposed mechanism in which the metal mediates electron transfer between the aromatic substrate and O<sub>2</sub> to form the semiquinone substrate radical-M(II)-superoxide (SQ<sup>•-</sup>-M<sup>II</sup>-O<sub>2</sub><sup>•-</sup>) reactive species. However, recent electron paramagnetic resonance (EPR) spectroscopic experiments demonstrated that a M(III)-superoxide complex was formed upon the O<sub>2</sub> binding to the enzyme–substrate (ES) complex of Mn-HPCD with HPCA<sup>6</sup> and Co-HPCD with the electron-poor substrate 4-nitrocatechol (4NC).<sup>9</sup> Therefore, the nature of reactive species and the reaction mechanism are yet to be elucidated. In this challenging endeavor, calculations, specially, quantum mechanical/molecular mechanical (QM/MM) calculations, can make significant contributions.

The iron-containing enzyme Fe-HPCD has been extensively studied by quantum mechanical (QM) and QM/MM methods.<sup>10–14</sup> In our previous QM/MM studies, a hybrid SQ<sup>•-</sup>-Fe<sup>II</sup>-O<sub>2</sub><sup>•-</sup>/Fe<sup>III</sup>-O<sub>2</sub><sup>•-</sup> was suggested to be the reactive species when native substrate HPCA was used,<sup>10</sup> while for the alternative substrate 4NC,<sup>11</sup> the Fe<sup>III</sup>-O<sub>2</sub><sup>•-</sup> species is the reactive one. Hence, the substrate was thought to play important roles in the dioxygen activation by Fe-HPCD. The QM studies of Mn-MndD by Siegbahn et al. indicated that the SQ<sup>•-</sup>-Mn<sup>II</sup>-O<sub>2</sub><sup>•-</sup> is the reactive species.<sup>15</sup> Compared to our knowledge of nonheme Fe(II)-containing enzymes, relative little is understood regarding the cobalt enzymes. It is still unclear that how dioxygen activation and extradiol cleavage carried out by the high-potential Co(II) center of Co-HPCD. To get more insight into the dioxygen activation and reaction mechanism of Co-HPCD, we investigated the reaction of this

Received: January 21, 2015

Revised: March 9, 2015

enzyme with the electron-rich substrate HPCA and the electron-poor substrate 4NC using the QM/MM approaches. As we should demonstrate, the reactive oxygen species is the doublet  $\text{Co}^{\text{III}}\text{-O}_2^{\bullet-}$  for Co-HPCD with 4NC and the quartet  $\text{SQ}^{\bullet}\text{-Co}^{\text{II}}\text{-O}_2^{\bullet-}$  species for Co-HPCD with HPCA.

## 2. COMPUTATIONAL METHODOLOGY

**2.1. QM/MM Methodology.** The chosen QM/MM methodology is analogous to that used in our previous studies for Fe-HPCD,<sup>10,11</sup> and therefore only the essential features are mentioned here. The  $\text{Co-O}_2$  adducts of the Co-HPCD were generated from the corresponding  $\text{Fe-O}_2$  adducts in our previous QM/MM study of the Fe-HPCD by replacing the iron by cobalt. All QM/MM calculations were carried out using ChemShell,<sup>16</sup> combining Turbomole<sup>17</sup> and DL\_POLY.<sup>18</sup> An electronic embedding scheme<sup>19</sup> was applied to include the polarizing effect of the enzymatic environment on the QM region. Hydrogen link atoms<sup>20</sup> with the charge shift model were used to treat the QM/MM boundary. Density functional theory (DFT) was used for the QM part, while the CHARMM<sup>21</sup> force field was used for the MM part. Geometry optimization was performed using the hybrid B3LYP<sup>22–24</sup> functional in combination with a double- $\zeta$  SV(P)<sup>25</sup> basis set (B1). The transition states (TSs) were determined as the highest point on the potential energy surface (PES) along the reaction coordinates, which were scanned with a small steps of 0.02 Å near the transition states. All QM/MM energy scans are collected in the Supporting Information (SI) document. The energies were corrected by single point calculations using a larger all-electron basis set B2, which is Def-TZVP<sup>26</sup> for all the atoms. In addition, the empirical dispersion correction was implemented in single point calculations by using the DFT-D3 program.<sup>27</sup> It was found that the dispersion corrections have only a minor effect on the relative energies of the key species in the reaction. Then the results are relegated to the SI.

It is well-known that predicting spin-state energetics correctly is a challenging subject in the transition-metal systems. In a study on the dioxygen activation of a Co(II) diketonate complex, the relative spin-state energetics of the cobalt–oxygen compound were found to be functional-sensitive (linear in the amount of exact exchange).<sup>28</sup> Recent studies suggest that the TPSSh<sup>29</sup> functional with 10% exact exchange is optimal for describing the energy of close-lying electronic states of a wide range of first-row transition metal systems.<sup>30,31</sup> Jensen et al. found that TPSSh achieves an unprecedented mean absolute error of ~11 kJ/mol in spin transition energies of the studied iron and cobalt complexes.<sup>32</sup> They pointed out that 10% exact exchange provides a proper balance between Fermi correlation effects on both sides of the reaction equation, hence, TPSSh is optimal for describing the electron correlation effects of the first-row transition metal systems. Therefore, we employed both B3LYP and TPSSh to evaluate the energetic by performing single-point calculations on the B3LYP-optimized geometries with the larger basis set B2. To explore the possible effect on geometries by the TPSSh functional, the geometry optimizations and PES scans were also performed using TPSSh(B1)/MM for Co-HPCD with HPCA. By comparison with the B3LYP(B1)/MM results, we found that the two types of functionals give similar geometries (see Figure S2 in the SI). Moreover, the relative energies at the TPSSh(B2)/MM//TPSSh(B1)/MM and TPSSh(B2)/MM//B3LYP(B1)/MM levels are very close. Specially, the difference in the barrier of the rate-limiting step is only 0.1 kcal/mol (Figure S4b vs Figure

7). As such, we focus here only the results from the single point calculations on the B3LYP-optimized geometries. Unless otherwise specified, the reported values are given at the B2 level.

**2.2. QM Region and Active Region.** The QM region, shown in Figure 1, comprises the first-coordination sphere

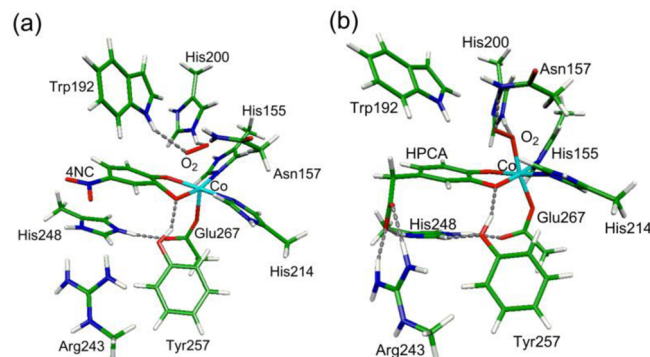


Figure 1. QM region for (a) Co-HPCD with 4NC and (b) Co-HPCD with HPCA.

residues, which are two histidines (His155 and His214), and substrate, and the second-coordination sphere residues (His200, His248, Trp192, Asn157, Tyr257, and Arg243). Histidines were modeled as methylimidazole, Glu267 as  $\text{CH}_3\text{COO}^-$ , Trp192 as indole, Asn157 as  $\text{CH}_3\text{CONH}_2$ , Arg243 as methylguanidinium, and Tyr257 as phenol. The active region for QM/MM geometry optimization included the core region (iron–oxygen and its first-coordination sphere) and all residues and water molecules within 6 Å from the core region. Details are given in the SI.

## 3. RESULTS

The coupling of triplet  $\text{O}_2$  with quartet  $\text{Co}^{\text{II}}$  gives rise to three possible spin states, the high-spin sextet, intermediate-spin quartet and low-spin doublet states. Here, all three spin-states were considered. So far, the  $\text{Co-O}_2$  adduct was not observed when the native substrate HPCA was used. However, a low-spin  $\text{Co}(\text{III})$ -superoxide complex was detected by a recent EPR spectroscopic experiment using the electron-poor substrate 4NC.<sup>9</sup> To validate our study, we first investigated the reaction mechanism of Co-HPCD with substrate 4NC (Co-HPCD/4NC). As shall be shown herein by means of hybrid QM/MM calculations, the  $\text{Co-O}_2$  adducts for Co-HPCD/4NC has doublet ground state with a  $\text{Co}(\text{III})$ -superoxide character, in good agreement with the EPR experiments. We then study the mechanism of Co-HPCD with HPCA (Co-HPCD/HPCA) using the same methods. Below we summarize our key results and findings, and the details of the results are relegated to the SI.

**3.1. Reaction of Co-HPCD with 4NC.** **3.1.1. Nature of the  $\text{Co-O}_2$  Adducts.** Figure 2 shows the electronic structure and relative energy of the various  $\text{Co-O}_2$  adducts for Co-HPCD with 4NC. Two different conformations (Figure 2a) were considered: In A1, the second-sphere His200 residue forms a hydrogen bond with the  $\text{OC}_2$  atom of the substrate. While in A2, His200 forms hydrogen bonds with the proximal oxygen of the  $\text{Co-O}_2$  moiety. Our results show that the doublet state having a  $\text{Co}^{\text{III}}\text{-O}_2^{\bullet-}$  character with the unique unpaired electron located on the  $\text{O}_2$  moiety is the ground state for both A1 and A2 conformations. This is consistent with the EPR experi-

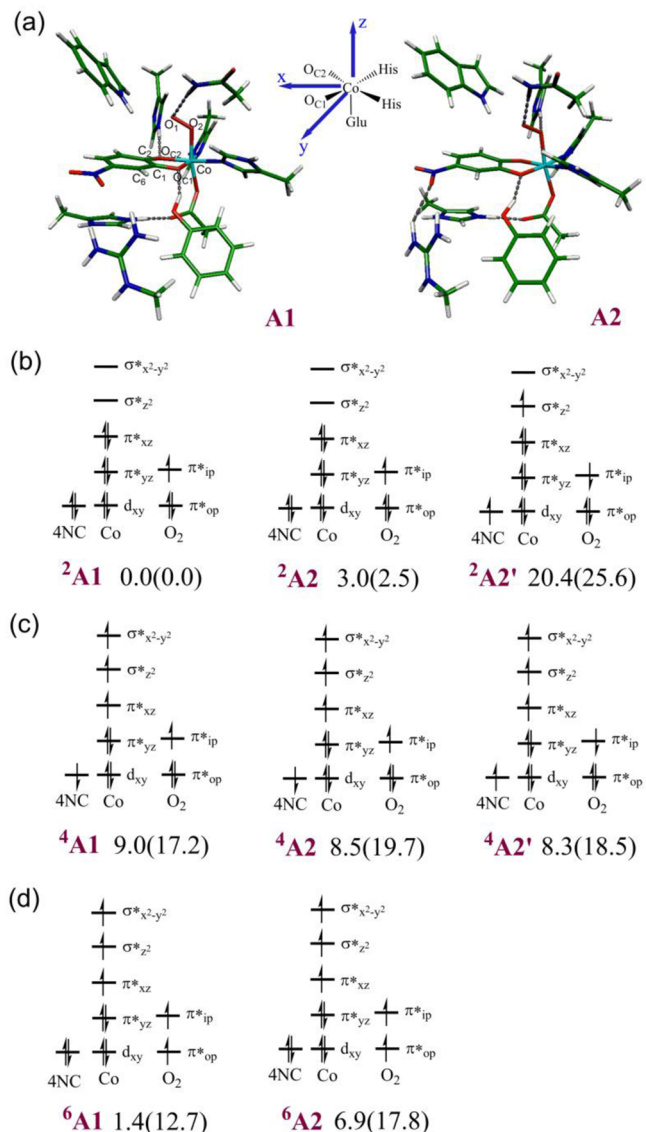


**Figure 2.** Co-O<sub>2</sub> adducts for Co-HPCD/4NC. (a) Two conformations of the Co-O<sub>2</sub> adducts. The electronic structures for the (b) the doublet states, (c) the quartet states, and (d) the sextet states. Relative energies are given in kcal/mol. The values out of parentheses are B3LYP(B2)/MM values, while in parentheses the values are at the TPSSh(B2)/MM level.

ments.<sup>9</sup> Moreover, a triradicaloid doublet state having  $SQ^{•\downarrow}\text{-Co}^{II}\text{-O}_2^{•-}$  character with the  $S = 1/2$  Co<sup>II</sup> center antiferromagnetically (AF) coupled to the superoxo radical (<sup>2</sup>A2' in Figure 2b) was also located and lies 20.4 kcal/mol above <sup>2</sup>A1 using B3LYP. All the quartet states were found to have  $SQ^{•\downarrow}\text{-Co}^{II}\text{-O}_2^{•-}$  character. Specifically, in <sup>4</sup>A1 and <sup>4</sup>A2, the substrate radical is AF coupled with the  $S = 3/2$  Co<sup>II</sup> center, labeled as  $SQ^{•\downarrow}\text{-Co}^{II}\text{-O}_2^{•-}$ , while in <sup>4</sup>A2', the superoxo radical is AF coupled with the metal center ( $SQ^{•\uparrow}\text{-Co}^{II}\text{-O}_2^{•-}$ ). Energetically, the quartet states are about 8–9 kcal/mol higher than <sup>2</sup>A1 using B3LYP, while this energy gap increases to 17–20 kcal/mol when TPSSh was applied. The sextet states involve a triplet ground state O<sub>2</sub> coupled ferromagnetically with a high-spin quartet Co(II). The optimized structures for the sextet state show that O<sub>2</sub> and the ES complex are not chemically bonded. <sup>6</sup>A1 and <sup>6</sup>A2 are 1.4 and 6.9 kcal/mol higher than the energy of <sup>2</sup>A1 at the B3LYP level.

**3.1.2. Reaction Mechanism for Co-HPCD with 4NC.** Due to the dissociation of the dioxygen in the sextet state of the adducts, we therefore investigated the reaction mechanism on the doublet and quartet potential energy surfaces. The computed mechanisms are depicted in Figure 3. The reaction pathways on the doublet surface described in Figure 3a are quite similar to that found for the Fe-HPCD.<sup>10</sup> The reaction starts with the dioxygen adduct, <sup>2</sup>A1, which undergoes a mere hydrogen bond reorientation of the His200 residue from interacting with the oxygen atom of the substrate ring, to hydrogen bonding with the proximal oxygen of the dioxygen moiety. The so-generated <sup>2</sup>A2 is the reactive oxygen species, in which the superoxide moiety attacks the substrate to form an alkylperoxo bridge species (<sup>2</sup>B). Consequently, the O–O bond is broken to yield <sup>2</sup>R, followed by the ring-closure for the epoxide formation (<sup>2</sup>E). After that, the reaction proceeds with the opening of the epoxide ring (<sup>2</sup>E → <sup>2</sup>L), a nucleophilic attack of the Co-bound OH on the carbonyl carbon C<sub>1</sub> (<sup>2</sup>L → <sup>2</sup>L-O), and the final scission of the ring to yield the semialdehyde product (<sup>2</sup>L-O → <sup>2</sup>P).

It can be seen from Figure 3b that the reaction pathway on the quartet surface involves three major steps. We noted that last two reaction steps, B → E and E → P, proceed through concerted mechanisms, which are different from the stepwise mechanism on the doublet surface. The opening of the O–O bond cleavage in <sup>4</sup>B coupled with the ring-closure to form an epoxide <sup>4</sup>E. For the last step, the opening of the epoxide ring, a nucleophilic attack of the Co-bound OH on the carbonyl carbon C<sub>1</sub>, and the final scission of the ring occurred jointly to yield the semialdehyde product (<sup>4</sup>E → <sup>4</sup>P).

The energy diagram for Co-HPCD with 4NC is shown in Figure 4. We found that at the B3LYP level the O–O bond cleavage of <sup>4</sup>A2, a  $SQ^{•\downarrow}\text{-Co}^{II}\text{-O}_2^{•-}$  species, have the lowest barrier compared with that for <sup>2</sup>A2 ( $\text{Co}^{III}\text{-O}_2^{•-}$ ) and <sup>4</sup>A2' ( $SQ^{•\uparrow}\text{-Co}^{II}\text{-O}_2^{•-}$ ), although the former species has higher energy. And the quartet alkylperoxo species (<sup>4</sup>B) is 7.8 kcal/mol lower in energy than the corresponding doublet state. However, when TPSSh was used, all the intermediates have doublet ground state. The quartet is preferred only at the final product stage. Nevertheless, both B3LYP and TPSSh predict a doublet ground state for the Co-O<sub>2</sub> adducts, in excellent agreement with the spectroscopic experiments.<sup>9</sup> And the rate-limiting step is the O–O bond cleavage with an accumulated barrier (relative to <sup>2</sup>A1) of 25.9/24.9 kcal/mol with B3LYP/B3LYP-D. Clearly, the B3LYP and B3LYP-D barriers are larger than the value of 19.9 kcal/mol calculated from the experimental rate constant (a rate constant of 0.72 min<sup>-1</sup> for  $[\text{Co-HPCD}(4\text{NC})\text{O}_2] \rightarrow \text{Co-HPCD} + \text{product}$ ),<sup>9</sup> whereas the TPSSh predicts an accumulated barrier of 21.5 kcal/mol for the rate-limiting step, in agreement with the experimental value.

**3.2. Reaction of Co-HPCD with HPCA.** **3.2.1. Co-O<sub>2</sub> Adducts for Co-HPCD/HPCA.** Due to the very rapid reaction of Co-HPCD with HPCA, the Co-O<sub>2</sub> adducts have not yet been detected. To get insight into the nature of the Co-O<sub>2</sub> adducts, we considered the doublet, quartet, and sextet spin states with two conformations (A1 and A2) having different hydrogen-bonding partners as in the case of Co-HPCD/4NC. The optimized structures for the doublet and quartet states of the Co-O<sub>2</sub> adducts are shown in Figure 5. Table 1 summarizes their spin densities and the relative energies. For the doublet states, besides the  $\text{Co}^{III}(S = 0)\text{-O}_2^{•-}$  species, <sup>2</sup>A1 and <sup>2</sup>A2, other three doublet states (<sup>2</sup>A2', <sup>2</sup>A2'', <sup>2</sup>A2''') were also located with the A2 conformation, in which His200 forms hydrogen

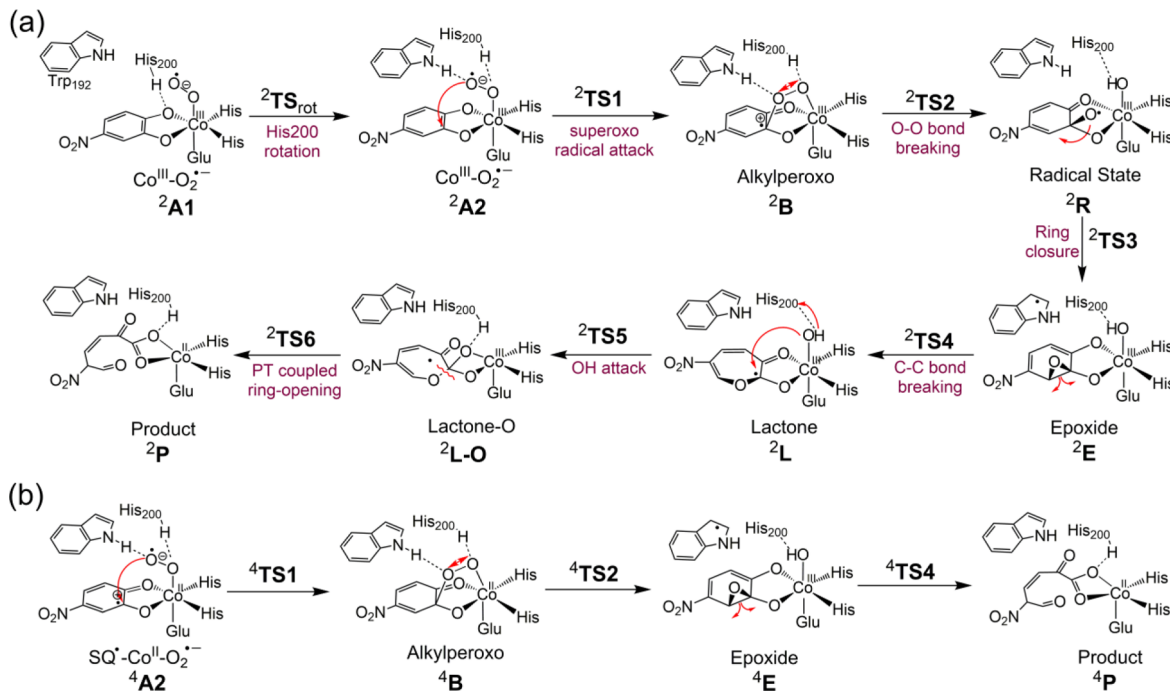


Figure 3. Reaction pathway on (a) the doublet surface and (b) the quartet surface for Co-HPCD with 4NC.

bonds with the proximal oxygen of the Co-O<sub>2</sub> moiety. Particularly, in <sup>2</sup>A2', the spin population is -0.02, 0.49, and 0.52 for Co, dioxygen, and the substrate, respectively. This electronic distribution can be interpreted as a partial electron transfer from HPCA to dioxygen of a Co<sup>III</sup>-O<sub>2</sub><sup>•-</sup> species. The calculated O–O bond length of the dioxygen moiety in <sup>2</sup>A2' (Figure Sf) is 1.37 Å, a value between those of metal-superoxide (~1.2–1.3 Å) and metal-peroxo compounds (~1.4–1.5 Å).<sup>33</sup> Hence, the electronic structure can be described as a mixture of Co<sup>III</sup>-O<sub>2</sub><sup>•-</sup> and SQ<sup>•</sup>-Co<sup>III</sup>-O<sub>2</sub><sup>2-</sup>. In addition, <sup>2</sup>A2'' and <sup>2</sup>A2''' were found to have SQ<sup>•</sup>-Co<sup>II</sup>(S = 1/2)-O<sub>2</sub><sup>•-</sup> character. <sup>2</sup>A2''<sub>HPCA</sub> involves a ferromagnetic coupling of the semiquinone substrate radical with the metal center (SQ<sup>•</sup><sup>↑</sup>-Co<sup>II</sup>-O<sub>2</sub><sup>•</sup><sup>↓</sup>), while <sup>2</sup>A2''' involves an antiferromagnetic coupling of the semiquinone substrate radical and the metal center (SQ<sup>•</sup><sup>↓</sup>-Co<sup>II</sup>-O<sub>2</sub><sup>•</sup><sup>↑</sup>). For the quartet states, <sup>4</sup>A1 and <sup>4</sup>A2 have SQ<sup>•</sup><sup>↑</sup>-Co<sup>II</sup>(S = 3/2)-O<sub>2</sub><sup>•</sup><sup>↑</sup> character, while <sup>4</sup>A1' is a Co<sup>III</sup>(S = 1)-O<sub>2</sub><sup>•</sup><sup>•-</sup> species, <sup>4</sup>A2' is a SQ<sup>•</sup><sup>↑</sup>-Co<sup>II</sup>(S = 3/2)-O<sub>2</sub><sup>•</sup><sup>↓</sup> species. The sextet states <sup>6</sup>A1 and <sup>6</sup>A2, in which all of the unpaired electrons have parallel spins, have SQ<sup>•</sup>-Co<sup>II</sup>(S = 3/2)-O<sub>2</sub><sup>•</sup><sup>•-</sup> character.

Energetically, one can see from Table 1 that the DFT functionals have a large effect on the spin-state energy ordering of the Co-O<sub>2</sub> adducts. With B3LYP, <sup>4</sup>A2' (SQ<sup>•</sup><sup>↑</sup>-Co<sup>II</sup>-O<sub>2</sub><sup>•</sup><sup>↓</sup>) has lowest energy, while TPSSh predicts a doublet ground state (Co<sup>III</sup>-O<sub>2</sub><sup>•</sup><sup>•-</sup>). It should be pointed out that the TPSSh(B2)/MM single point calculations for <sup>2</sup>A2'' and <sup>2</sup>A2''' all failed since their electronic configuration invariably change to the Co<sup>III</sup>-O<sub>2</sub><sup>•</sup><sup>•-</sup> state. Moreover, A1 and A2 can interconvert rapidly by reorientation of His200. The barrier for the formation of <sup>2</sup>A2 from <sup>2</sup>A1 is 5.3/4.5 kcal/mol with B3LYP/TPSSh, whereas the formation of <sup>4</sup>A2 from <sup>4</sup>A1 is barrier-free.

**3.2.2. Reaction Mechanism for Co-HPCD with HPCA.** The reaction pathways of Co-HPCD with HPCA were depicted in Figure 6. Energetics along the pathways are shown in Figure 7. The catalytic reaction of Co-HPCD with HPCA involves three major steps. Similar to the proposed mechanism for Co-

HPCD/4NC, the first major step is the attack of the superoxide moiety of A2 on the substrate to form an alkylperoxo bridge species. The second phase involves the O–O bond cleavage of the bridge species and the ring-closure for the epoxide formation (E). Finally, the reaction proceeded through the opening of the epoxide ring, a nucleophilic attack of the Co-bound OH on the carbonyl carbon C<sub>1</sub>, and the final scission of the ring to yield the semialdehyde product. The detailed discussion of the mechanism and the calculated energetic is presented in the following subsections.

**Attack of the Superoxide.** After the formation of the dioxygen adducts, the next step is the attack of the superoxide on the substrate to form the alkylperoxo bridge species. The reaction from sextet states is unfavorable due to their SQ<sup>•</sup>-Co<sup>II</sup>(S = 3/2)-O<sub>2</sub><sup>•</sup><sup>•-</sup> character with five unpaired parallel spins. Indeed, here we found that the energy keeps increasing during the attack from <sup>6</sup>A2 (see Figure S20). Since the precise reactive species (Co<sup>III</sup>-superoxide or semiquinone-Co<sup>II</sup>-superoxide) is still unclear, we therefore studied the superoxide radical attack on the substrate C<sub>1</sub> atom starting from all the doublet and quartet A2 species. It was found that the superoxide attack for the Co<sup>III</sup>-O<sub>2</sub><sup>•</sup><sup>•-</sup> species (<sup>2</sup>A2) is a two-electron oxidation process coupled with proton transfer from His200 to the proximal oxygen of the dioxygen moiety, resulting in the formation of the low spin Co<sup>II</sup> (S = 1/2) alkylperoxo species (<sup>2</sup>B), while for the hybrid Co<sup>III</sup>-O<sub>2</sub><sup>•</sup><sup>•-</sup>/SQ<sup>•</sup>-Co<sup>III</sup>-O<sub>2</sub><sup>2-</sup> (<sup>2</sup>A2'), electron transfer from the substrate to the dioxygen moiety occurred to yield a semiquinone-Co<sup>III</sup>-alkylperoxo species (<sup>2</sup>B'). The transition states (TSs) leading from <sup>2</sup>A2 (<sup>2</sup>A2') to <sup>2</sup>B (<sup>2</sup>B') are designated <sup>2</sup>TS1 (<sup>2</sup>TS1'). Starting from <sup>2</sup>A2'' and <sup>2</sup>A2''', the energy scans collapse to the potential energy surface of <sup>2</sup>A2' (see Figure 8a). For the quartet SQ<sup>•</sup>-Co<sup>II</sup>-O<sub>2</sub><sup>•</sup><sup>•-</sup> species (<sup>4</sup>A2 and <sup>4</sup>A2'), the radical character of the substrate and dioxygen moiety is quenched to form the high spin Co<sup>II</sup> (S = 3/2) alkylperoxo species (<sup>4</sup>B) via <sup>4</sup>TS1 and <sup>4</sup>TS1', respectively. It can be seen from Figure 7 that <sup>4</sup>TS1' has the lowest energy compared with other TSs for the formation of the alkylperoxo species with

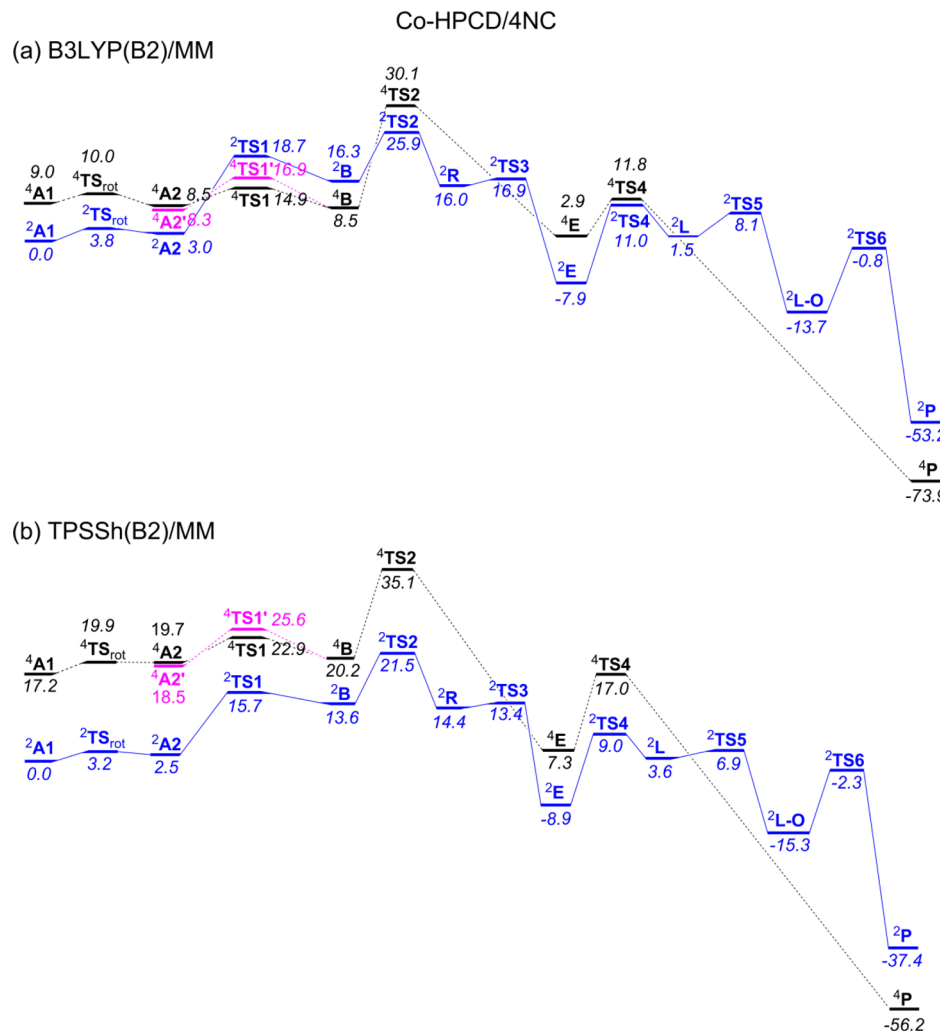


**Figure 4.** Energy profile for Co-HPCD with 4NC at (a) B3LYP(B2)/MM and (b) TPSSh(B2)/MM levels. All energies are in kcal/mol.

either B3LYP or TPSSh. As such, the quartet  $\text{SQ}^{\bullet+}\text{-Co}^{\text{II}}\text{-O}_2^{\bullet-}$  species ( ${}^4\text{A}2'$ ) is the reactive dioxygen adducts. Moreover,  ${}^4\text{B}$  has the lowest energy among the alkylperoxo species.  ${}^2\text{B}$  and  ${}^2\text{B}'$  lie 13.1/10.7 and 21.3/6.6 kcal/mol above  ${}^4\text{B}$  with B3LYP/TPSSh.

**O–O Bond Cleavage and Formation of the Epoxide.** After the formation of the alkylperoxo species, the next step is the O–O bond cleavage. The calculations show that the O–O bond cleavage of the quartet  $\text{Co}^{\text{II}}(S = 3/2)$ -alkylperoxo species takes place with the simultaneous formation of the C–O bond to yield the epoxide species ( ${}^4\text{E}$  and  ${}^4\text{E}'$  in Figure 6b).  ${}^4\text{E}$  is a complex of  $\text{Co}^{\text{III}}(S = 2)$ -OH with a substrate epoxide (SE) radical, whereas  ${}^4\text{E}'$  is a triradicaloid  $\text{SE}^{\bullet+}\text{-Co}^{\text{III}}(S = 1)$ -OH species. The calculated barrier for  ${}^4\text{B} \rightarrow {}^4\text{E}$  is 19.9/13.6 kcal/mol with B3LYP/TPSSh, which is lower than that for  ${}^4\text{B} \rightarrow {}^4\text{E}'$  (27.0/16.8 kcal/mol with B3LYP/TPSSh).  ${}^4\text{E}'$  is 5.1/7.0 kcal/mol more stable than  ${}^4\text{E}$  at the B3LYP/TPSSh level, whereas for the doublet states, the mechanism is stepwise. Starting from  ${}^2\text{B}$ , the O–O bond cleavage coupled with electron transfer from Co to the peroxy group leads to a complex of  $\text{Co}^{\text{III}}(S = 1)$ -OH with a gem-diol radical ( ${}^2\text{R}$ ), which collapses in a barrier-free manner to a triradicaloid  $\text{SE}^{\bullet+}\text{-Co}^{\text{III}}(S = 1)$ -OH species ( ${}^2\text{E}$ ). For  ${}^2\text{B}'$ , the O–O bond cleavage is coupled with proton transfer from His200 to proximal oxygen. The resultant  ${}^2\text{R}'$  contained  $\text{Co}^{\text{III}}(S = 0)$ -OH, as well as an unprotonated

gem-diol. The subsequent C–O bond formation has a small energy barrier (3.7/2.8 kcal/mol at the B3LYP/TPSSh level). The so-generated  ${}^2\text{E}'$  has lowest energy compared with  ${}^2\text{E}$  and the corresponding quartet states ( ${}^4\text{E}$  and  ${}^4\text{E}'$ ).

**Completion Steps of the Reaction.** After the formation of the epoxide intermediate, the reaction proceeds with ring-opening ( $\text{C}_1\text{-C}_6$  bond cleavage), attack of OH on  $\text{C}_1$ , and then again ring-opening through  $\text{C}_1\text{-O}_1$  bond breaking to yield the semialdehyde product. For the doublet states, the process is stepwise (Figure 6a). Opening of the epoxide ring for  ${}^2\text{E}$  leads to a  $\text{Co}^{\text{III}}(S = 1)$ -OH bounded lactone radical species ( ${}^2\text{L}$ ), followed by the attack of the hydroxyl group on lactone to form  ${}^2\text{L-OH}$ . Starting from  ${}^2\text{E}'$ , opening of the epoxide ring results in the formation of a  $\text{Co}^{\text{III}}(S = 0)$ -OH bounded lactone radical species ( ${}^2\text{L}'$ ), in which the hydroxyl group can attack the lactone radical to yield  ${}^2\text{L-OH}'$ . Both  ${}^2\text{L-OH}$  and  ${}^2\text{L-OH}'$  undergo ring-opening process to give the product ( ${}^2\text{P}$ ). For the quartet states ( ${}^4\text{E}$  and  ${}^4\text{E}'$ ), the opening of the epoxide ring is coupled with attack of Co-bounded OH on  $\text{C}_1$  to generate  ${}^4\text{L-OH}$ , which undergoes ring-opening process to give the final product ( ${}^4\text{P}$ ).

**3.2.3. Energetics of the Reaction.** Figure 7a shows the B3LYP results. It is seen that  ${}^4\text{A}2'$  is the reactive oxygen species for Co-HPCD/HPCA and the rate-limiting step is the O–O bond cleavage of the alkylperoxo bridge species ( ${}^4\text{B} \rightarrow {}^4\text{E}$ ) with

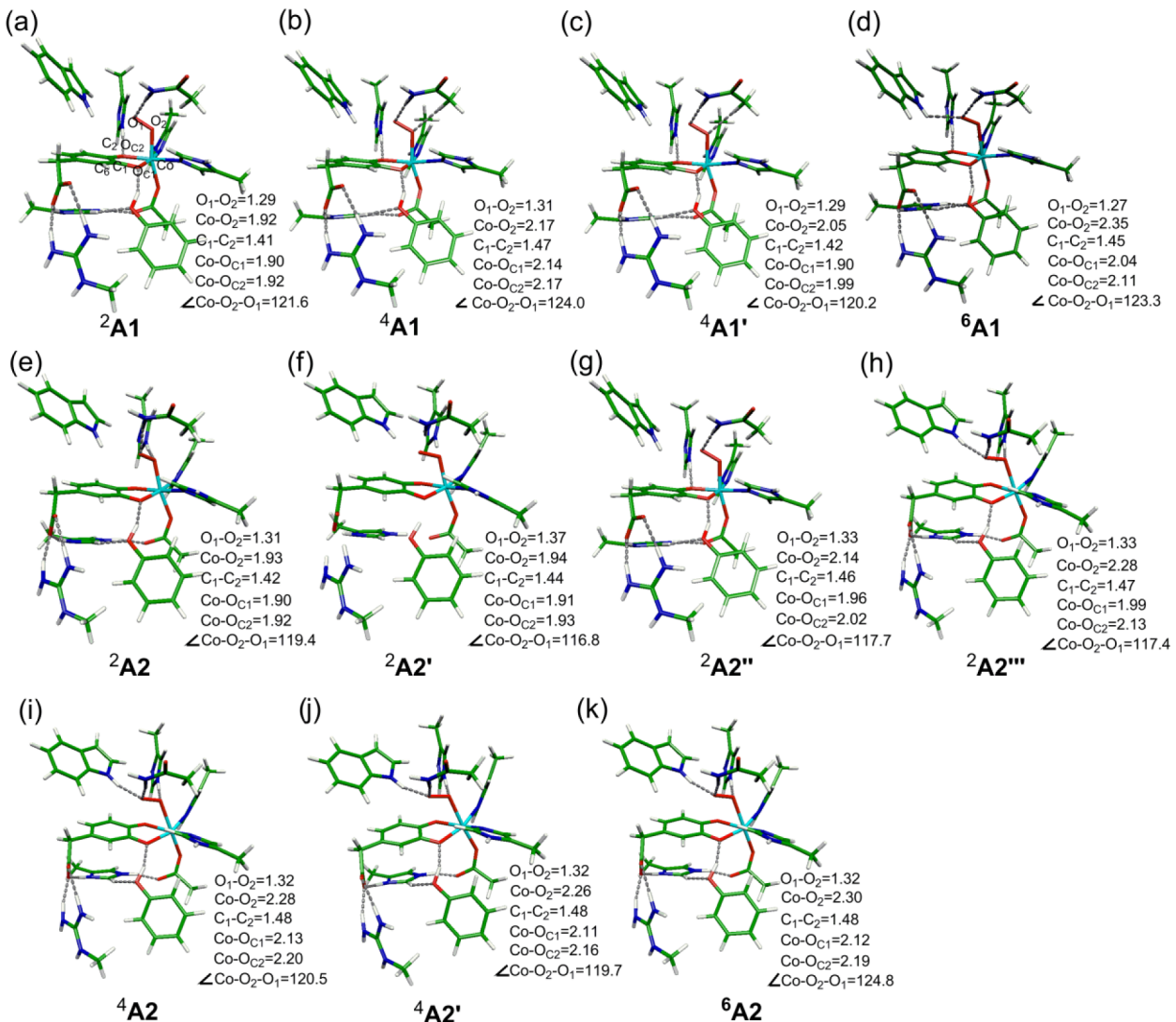


**Figure 5.** Optimized structures of the doublet and quartet Co-O<sub>2</sub> adducts for Co-HPCD/HPCA. All distances are in Å, while angles are in degrees.

**Table 1. Relative Energies and Spin Densities of the Co-O<sub>2</sub> Adducts of HPCD with the Native Substrate HPCA**

species	$\Delta E$ (kcal/mol)		spin densities <sup>a</sup>						
	B3LYP	TPSSh	Co	O <sub>1</sub>	O <sub>2</sub>	O <sub>C1</sub>	O <sub>C2</sub>	sub <sup>b</sup>	L <sup>c</sup>
<sup>2</sup> A1(Co <sup>III</sup> -O <sub>2</sub> <sup>•-</sup> )	0.0	0.0	-0.08	0.58	0.47	0.01	0.01	0.02	0.00
<sup>4</sup> A1(SQ <sup>•+</sup> -Co <sup>II</sup> -O <sub>2</sub> <sup>•-</sup> )	2.9	14.6	2.77	0.45	0.48	-0.15	-0.13	-0.81	0.11
<sup>4</sup> A1'(Co <sup>III</sup> -O <sub>2</sub> <sup>•-</sup> )	12.8	12.4	1.76	0.55	0.49	-0.03	0.13	0.14	0.05
<sup>6</sup> A1(SQ <sup>•+</sup> -Co <sup>II</sup> -O <sub>2</sub> <sup>•-</sup> )	0.7	11.6	2.78	0.71	0.72	0.17	0.15	0.67	0.03
<sup>2</sup> A2(Co <sup>III</sup> -O <sub>2</sub> <sup>•-</sup> )	4.7	4.0	-0.04	0.58	0.35	0.01	0.04	0.10	0.00
<sup>2</sup> A2'(Co <sup>III</sup> -O <sub>2</sub> <sup>•-</sup> /SQ <sup>•+</sup> -Co <sup>III</sup> -O <sub>2</sub> <sup>2-</sup> )	5.5	3.9	-0.02	0.35	0.14	0.06	0.12	0.52	0.00
<sup>2</sup> A2''(SQ <sup>•+</sup> -Co <sup>II</sup> -O <sub>2</sub> <sup>•-</sup> )	8.0		0.84	-0.43	-0.32	0.15	0.21	0.88	-0.02
<sup>2</sup> A2'''(SQ <sup>•+</sup> -Co <sup>II</sup> -O <sub>2</sub> <sup>•-</sup> )	13.3		0.92	0.51	0.36	-0.15	-0.17	-0.82	0.01
<sup>4</sup> A2(SQ <sup>•+</sup> -Co <sup>II</sup> -O <sub>2</sub> <sup>•-</sup> )	0.5	14.5	2.78	0.51	0.38	-0.12	-0.17	-0.80	0.12
<sup>4</sup> A2'(SQ <sup>•+</sup> -Co <sup>II</sup> -O <sub>2</sub> <sup>•-</sup> )	-3.6	7.7	2.76	-0.52	-0.35	0.19	0.24	0.96	0.12
<sup>6</sup> A2(SQ <sup>•+</sup> -Co <sup>II</sup> -O <sub>2</sub> <sup>•-</sup> )	0.6	12.7	2.81	0.58	0.43	0.21	0.28	1.04	0.03

<sup>a</sup>The spin density at the B3LYP(B1)/MM level. <sup>b</sup>The spin density for O<sub>C1</sub> and O<sub>C2</sub> are also included for the substrate. <sup>c</sup>The ligated N atoms of His155, His214, and O atom of Glu267.

a barrier of 19.9 kcal/mol at the B3LYP level (19.0 kcal/mol at the B3LYP-D level in Figure S4a). Apparently, this value is higher than the estimated one (15.5 kcal/mol) from the experiment (rate constant of 1120 min<sup>-1</sup>) where the rate-

limiting step was suggested to occur in the O<sub>2</sub> binding and activation phase.<sup>7</sup> It is indicated again that B3LYP overestimates the reaction barrier as in the case of Co-HPCD/4NC. We note that at the TPSSh/MM level the doublet <sup>2</sup>A2' has

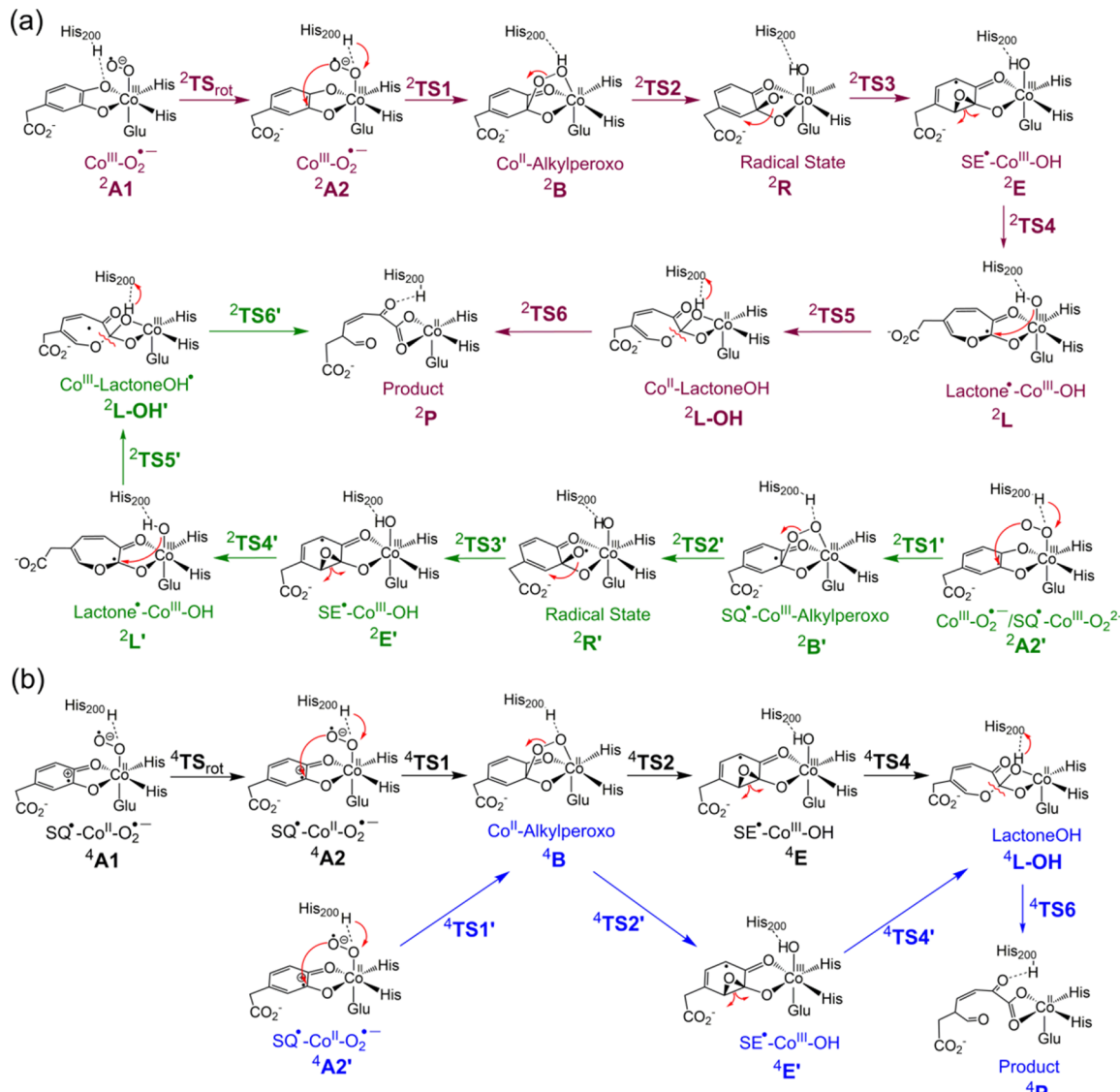


Figure 6. Reaction pathway on (a) the doublet surface and (b) the quartet surface for Co-HPCD with HPCA.

lowest energy compared with other  $\text{Co-O}_2$  adducts, but  $^4\text{A}2'$  is the state that correlates to the lowest TS of the superoxo attack. It is possible that the spin transition from the doublet to the quartet occurs before reaching the TS of the superoxo attack. And the transition between the doublet and quartet states could also occur in the O–O bond cleavage and the formation of L-OH species. Overall, TPSSh/MM predicts an accumulated barrier of 12.0 kcal/mol for the rate-limiting O–O bond cleavage step. This value is lower than the experimental value for the  $\text{O}_2$  binding and activation phase. Hence, we can conclude that TPSSh/MM gives reasonable results.

#### 4. DISCUSSION

**4.1. Effects of Substrate on Reaction Mechanism.** We discuss here the effects of substrate on reaction mechanism based on the energy profile obtained from the TPSSh/MM calculations (Figures 4b and 7b). As shown in Figure 4b, the reaction takes place via the doublet surface for Co-HPCD/4NC producing the doublet product ( $^2\text{P}$ ), which converts to the quartet product  $^4\text{P}$  upon spin transition. For Co-HPCD/HPCA (Figure 7b), the interchanges of spin states were observed in

the superoxo attack, O–O bond breaking, and L-OH formation steps. In both cases, the rate-limiting step is the O–O bond cleavage step. The barrier for this step is 21.5 kcal/mol for Co-HPCD/4NC, which is higher than that for Co-HPCD/HPCA (12.0 kcal/mol). It is interesting to note that the reactive oxygen species is different when different substrate was used. For the electron-poor substrate 4NC, the reactive oxygen species is the  $\text{Co}^{\text{III}}\text{-O}_2^{\bullet-}$  species. For the electron-rich substrate HPCA (Figure 7b), it is the quartet  $\text{SQ}^{\bullet}\text{-Co}^{\text{II}}\text{-O}_2^{\bullet-}$  species. This finding is quite similar to that found in Fe-HPCD.<sup>10,11</sup> Therefore, our QM/MM studies for Co-HPCD highlight once again the important role of the substrate on the dioxygen activation and reaction mechanism of extradiol dioxygenases.

**4.2. Comparison with Fe-HPCD.** Previously, we used the QM/MM methods to study the reaction mechanism of Fe-HPCD with HPCA and 4NC.<sup>10,11</sup> It is interesting to compare Fe-HPCD and its cobalt-substituted congener (Co-HPCD) considered here. First, we compare the reactive oxygen species in the different systems. It was found that when the electron-deficient substrate 4NC was used, the  $\text{M}^{\text{III}}\text{-O}_2^{\bullet-}$  species is reactive oxygen species in both Fe-HPCD and Co-HPCD. On the other hand, the electron-rich substrate HPCA can donate

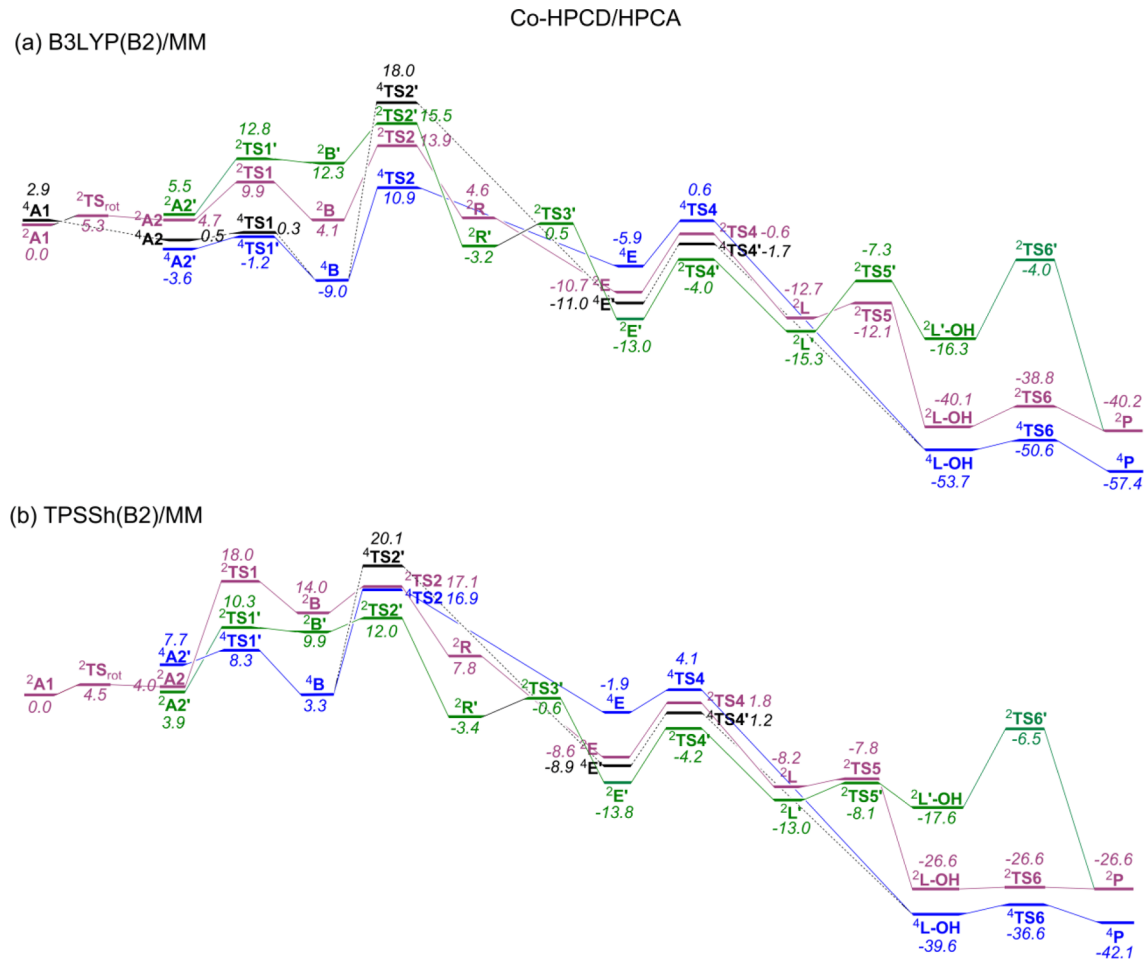


Figure 7. Energy profile for Co-HPCD with HPCA at (a) B3LYP(B2)/MM and (b) TPSSh(B2)/MM levels.

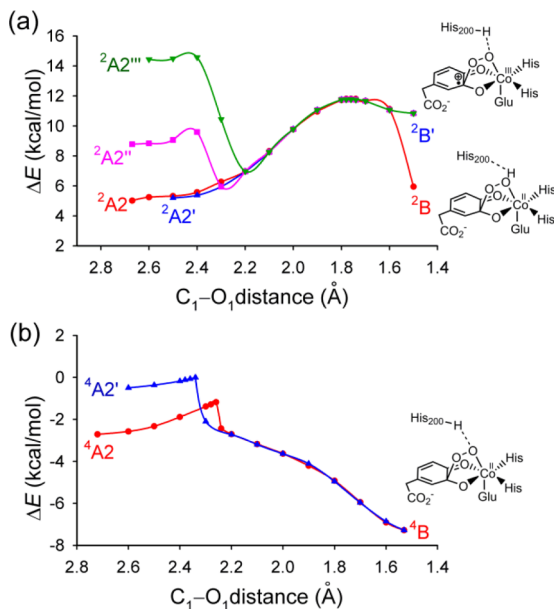


Figure 8. B3LYP(B1)/MM energy profile along the forming O<sub>2</sub>-C<sub>1</sub> bond starting from (a) the doublet states and (b) the quartet states of the Co-O<sub>2</sub> adducts.

electron density. For Fe-HPCD, only partial electron transfer from HPCA occurs and the so-generated hybrid Fe<sup>III</sup>-O<sub>2</sub><sup>•-</sup>/SQ<sup>•</sup>-Fe<sup>II</sup>-O<sub>2</sub><sup>•-</sup> species is the reactive species, while for Co-

HPCD, SQ<sup>•</sup>-Co<sup>II</sup>-O<sub>2</sub><sup>•-</sup> is the reactive one. Another interesting aspect is the rate-limiting step. For Fe-HPCD, the rate-limiting step is the attack of the superoxo group on the substrate for 4NC, and the O–O bond cleavage for HPCA. For Co-HPCD, the rate-limiting step is the O–O bond cleavage step for both 4NC and HPCA.

## 5. CONCLUSION

We presented here QM/MM calculations of the reaction mechanism of Co-HPCD with the electron-rich substrate HPCA and electron-poor substrate 4NC. Our results demonstrated that the Co-O<sub>2</sub> adducts has doublet ground state with a Co<sup>III</sup>-O<sub>2</sub><sup>•-</sup> character when 4NC was used as the substrate, in good agreement with the EPR spectroscopic experiment. The reaction takes place via the doublet surface with the doublet Co<sup>III</sup>-O<sub>2</sub><sup>•-</sup> being the reactive species. On the other hand, the DFT functional used in the QM part was found to have a large effect on the relative energies of the doublet and quartet states in the case of Co-HPCD/HPCA. Specially, B3LYP predicts a quartet (SQ<sup>•</sup><sup>+</sup>-Co<sup>II</sup>-O<sub>2</sub><sup>•-</sup>) ground state for the Co-O<sub>2</sub> adducts, while TPSSh predicts a doublet Co<sup>III</sup>-O<sub>2</sub><sup>•-</sup> ground state. The quartet SQ<sup>•</sup><sup>+</sup>-Co<sup>II</sup>-O<sub>2</sub><sup>•-</sup> species is the reactive species for Co-HPCD/HPCA. B3LYP was found to overestimate the reaction barrier for both Co-HPCD/4NC and Co-HPCD/HPCA. TPSSh predicts barriers of 21.5 versus 12.0 kcal/mol for Co-HPCD/4NC versus Co-HPCD/HPCA, in line

with the fact that the rate of the reaction is decreased when the substrate was changed from HPCA to 4NC.

## ASSOCIATED CONTENT

### Supporting Information

The MM optimized region and a full set of computational results. This material is available free of charge via the Internet at <http://pubs.acs.org>.

## AUTHOR INFORMATION

### Corresponding Author

\*E-mail: wenzhenlai@ruc.edu.cn.

### Notes

The authors declare no competing financial interest.

## ACKNOWLEDGMENTS

This work is supported by the Fundamental Research Funds for the Central Universities, the Research Funds of Renmin University of China (Program No. 12XNLJ04), and the National Natural Science Foundation of China (No. 21203245).

## REFERENCES

- (1) Smith, M. R. The Biodegradation of Aromatic Hydrocarbons by Bacteria. *Biodegradation* **1990**, *1*, 191–206.
- (2) Koehntop, K. D.; Emerson, J. P.; Que, L., Jr. The 2-His-1-Carboxylate Facial Triad: A Versatile Platform for Dioxygen Activation by Mononuclear Non-Heme Iron(II) Enzymes. *J. Biol. Inorg. Chem.* **2005**, *10*, 87–93.
- (3) Bruijninx, P. C. A.; van Koten, G.; Gebbink, R. Mononuclear Non-Heme Iron Enzymes with the 2-His-1-Carboxylate Facial Triad: Recent Developments in Enzymology and Modeling Studies. *Chem. Soc. Rev.* **2008**, *37*, 2716–2744.
- (4) Vetting, M. W.; Wackett, L. P.; Que, L., Jr.; Lipscomb, J. D.; Ohlendorf, D. H. Crystallographic Comparison of Manganese- and Iron-Dependent Homoprotocatechuate 2,3-Dioxygenases. *J. Bacteriol.* **2004**, *186*, 1945–1958.
- (5) Emerson, J. P.; Kovaleva, E. G.; Farquhar, E. R.; Lipscomb, J. D.; Que, L., Jr. Swapping Metals in Fe- and Mn-Dependent Dioxygenases: Evidence for Oxygen Activation without a Change in Metal Redox State. *Proc. Natl. Acad. Sci. U.S.A.* **2008**, *105*, 7347–7352.
- (6) Gunderson, W. A.; Zatsman, A. I.; Emerson, J. P.; Farquhar, E. R.; Que, L., Jr.; Lipscomb, J. D.; Hendrich, M. P. Electron Paramagnetic Resonance Detection of Intermediates in the Enzymatic Cycle of an Extradiol Dioxygenase. *J. Am. Chem. Soc.* **2008**, *130*, 14465–14467.
- (7) Fielding, A. J.; Kovaleva, E. G.; Farquhar, E. R.; Lipscomb, J. D.; Que, L. A Hyperactive Cobalt-Substituted Extradiol-Cleaving Catechol Dioxygenase. *J. Biol. Inorg. Chem.* **2011**, *16*, 341–355.
- (8) Bratsch, S. G. Standard Electrode Potentials and Temperature Coefficients in Water at 298.15 K. *J. Phys. Chem. Ref. Data* **1989**, *18*, 1–21.
- (9) Fielding, A. J.; Lipscomb, J. D.; Que, L., Jr. Characterization of an O<sub>2</sub> Adduct of an Active Cobalt-Substituted Extradiol-Cleaving Catechol Dioxygenase. *J. Am. Chem. Soc.* **2012**, *134*, 796–799.
- (10) Dong, G.; Shaik, S.; Lai, W. Z. Oxygen Activation by Homoprotocatechuate 2,3-Dioxygenase: A QM/MM Study Reveals the Key Intermediates in the Activation Cycle. *Chem. Sci.* **2013**, *4*, 3624–3635.
- (11) Dong, G.; Lai, W. Z. Reaction Mechanism of Homoprotocatechuate 2,3-Dioxygenase with 4-Nitrocatechol: Implications for the Role of Substrate. *J. Phys. Chem. B* **2014**, *118*, 1791–1798.
- (12) Christian, G. J.; Ye, S. F.; Neese, F. Oxygen Activation in Extradiol Catecholate Dioxygenases: A Density Functional Study. *Chem. Sci.* **2012**, *3*, 1600–1611.
- (13) Siegbahn, P. E. M.; Haefner, F. Mechanism for Catechol Ring-Cleavage by Non-Heme Iron Extradiol Dioxygenases. *J. Am. Chem. Soc.* **2004**, *126*, 8919–8932.
- (14) Georgiev, V.; Borowski, T.; Blomberg, M. R. A.; Siegbahn, P. E. M. A Comparison of the Reaction Mechanisms of Iron- and Manganese-Containing 2,3-HPCD: An Important Spin Transition for Manganese. *J. Biol. Inorg. Chem.* **2008**, *13*, 929–940.
- (15) Georgiev, V.; Borowski, T.; Siegbahn, P. E. M. Theoretical Study of the Catalytic Reaction Mechanism of MndD. *J. Biol. Inorg. Chem.* **2006**, *11*, 571–585.
- (16) Sherwood, P.; de Vries, A. H.; Guest, M. F.; Schreckenbach, G.; Catlow, C. R. A.; French, S. A.; Sokol, A. A.; Bromley, S. T.; Thiel, W.; Turner, A. J.; et al. QUASI: A General Purpose Implementation of the QM/MM Approach and Its Application to Problems in Catalysis. *J. Mol. Struct.: THEOCHEM* **2003**, *632*, 1–28.
- (17) TURBOMOLE, version 6.4; TURBOMOLE GmbH: Karlsruhe, Germany, 2012.
- (18) Smith, W.; Forester, T. R. DL\_POLY\_2.0: A General-Purpose Parallel Molecular Dynamics Simulation Package. *J. Mol. Graphics* **1996**, *14*, 136–141.
- (19) Bakowies, D.; Thiel, W. Hybrid Models for Combined Quantum Mechanical and Molecular Mechanical Approaches. *J. Phys. Chem.* **1996**, *100*, 10580–10594.
- (20) de Vries, A. H.; Sherwood, P.; Collins, S. J.; Rigby, A. M.; Rigo, M.; Kramer, G. J. Zeolite Structure and Reactivity by Combined Quantum-Chemical–Classical Calculations. *J. Phys. Chem. B* **1999**, *103*, 6133–6141.
- (21) MacKerell, A. D.; Bashford, D.; Bellott, M.; Dunbrack, R. L.; Evanseck, J. D.; Field, M. J.; Fischer, S.; Gao, J.; Guo, H.; Ha, S.; et al. All-Atom Empirical Potential for Molecular Modeling and Dynamics Studies of Proteins. *J. Phys. Chem. B* **1998**, *102*, 3586–3616.
- (22) Becke, A. D. Density-Functional Exchange-Energy Approximation with Correct Asymptotic Behavior. *Phys. Rev. A* **1988**, *38*, 3098–3100.
- (23) Lee, C.; Yang, W.; Parr, R. G. Development of the Colle-Salvetti Correlation-Energy Formula into a Functional of the Electron Density. *Phys. Rev. B* **1988**, *37*, 785–789.
- (24) Becke, A. D. Density-Functional Thermochemistry. III. The Role of Exact Exchange. *J. Chem. Phys.* **1993**, *98*, 5648–5652.
- (25) Schäfer, A.; Horn, H.; Ahlrichs, R. Fully Optimized Contracted Gaussian Basis Sets for Atoms Li to Kr. *J. Chem. Phys.* **1992**, *97*, 2571–2577.
- (26) Schäfer, A.; Huber, C.; Ahlrichs, R. Fully Optimized Contracted Gaussian Basis Sets of Triple Zeta Valence Quality for Atoms Li to Kr. *J. Chem. Phys.* **1994**, *100*, 5829–5835.
- (27) Grimme, S.; Antony, J.; Ehrlich, S.; Krieg, H. A Consistent and Accurate Ab Initio Parametrization of Density Functional Dispersion Correction (DFT-D) for the 94 Elements H–Pu. *J. Chem. Phys.* **2010**, *132* (154104), 1–19.
- (28) Kubas, A.; Hartung, J.; Fink, K. How Molecular Oxygen Binds to Bis [trifluoroacetylacetone(-)]cobalt(II): Ab Initio and Density Functional Theory Studies. *Dalton Trans.* **2011**, *40*, 11289–11295.
- (29) Tao, J. M.; Perdew, J. P.; Staroverov, V. N.; Scuseria, G. E. Climbing the Density Functional Ladder: Nonempirical Meta-Generalized Gradient Approximation Designed for Molecules and Solids. *Phys. Rev. Lett.* **2003**, *91* (146401), 1–4.
- (30) Jensen, K. P. Bioinorganic Chemistry Modeled with the TPSSh Density Functional. *Inorg. Chem.* **2008**, *47*, 10357–10365.
- (31) Kepp, K. P. The Ground States of Iron(III) Porphines: Role of Entropy-Enthalpy Compensation, Fermi Correlation, Dispersion, and Zero-Point Energies. *J. Inorg. Biochem.* **2011**, *105*, 1286–1292.
- (32) Jensen, K. P.; Cirera, J. Accurate Computed Enthalpies of Spin Crossover in Iron and Cobalt Complexes. *J. Phys. Chem. A* **2009**, *113*, 10033–10039.
- (33) Perdew, J. P. Density-Functional Approximation for the Correlation-Energy of the Inhomogeneous Electron-Gas. *Phys. Rev. B* **1986**, *33*, 8822–8824.